Theor Chem Account (2008) 119:143–153
DOI 10.1007/s00214-007-0298-2

REGULAR ARTICLE

Regional organic geochemistry of host sediments of Palaeoproterozoic McArthur River Ore deposit, Australia

Karen L. Mackenzie · Craig P. Marshall · Malcolm R. Walter

Received: 5 June 2006 / Accepted: 2 April 2007 / Published online: 26 May 2007

Abstract The 1,640 Ma HYC (Here's Your Chance) deposit at McArthur River, Northern Territory, Australia, is one of the largest and least metamorphosed Proterozoic stratiform lead-zinc-silver deposits in the world. The thermal history of the deposit is a currently not well understood, both low and high temperature mechanisms have been proposed. From our study we were able to estimate (from both kerogen and bitumen thermal maturity indices which concur) the thermal maturity to be equivalent to Ro 1.1–2.0%, corresponding to the wet gas generation zone, with a maximum relatively low burial temperature range of 120–180 °C in the ore samples. Regionally, temperatures were not further constrained due to the complex and dynamic nature of the sedimentary environment.

Contribution to the P.J. Stephens 65th Birthday Festschrift Issue.

K. L. Mackenzie
School of Geosciences, University of Sydney,
Sydney, NSW 2006, Australia

K. L. Mackenzie (✉)
Water and Environment Business Unit,
Sinclair Knight Merz, 263, Adelaide Terrace,
Perth, WA 6000, Australia
e-mail: peterandkaren47b@bigpond.com

C. P. Marshall · M. R. Walter
Australian Centre for Astrobiology,
Department of Earth and Planetary Sciences,
Macquarie University, Sydney, NSW 2109, Australia

Present Address:
C. P. Marshall
School of Chemistry, University of Sydney,
Sydney, NSW 2006, Australia

Keywords Hydrothermal · Bitumen · Mineralisation · Kerogen · Raman spectroscopy

1 Introduction

Palaeoproterozoic rocks of northern Australia contain numerous sediment-hosted stratiform lead-zinc-silver deposits including Mount Isa and McArthur River (also known as HYC). The 1,640 Ma HYC (a contraction of the expression, "Here's your chance'') deposit at McArthur River, Northern Territory, Australia, is one of the largest and least metamorphosed stratiform lead-zinc-silver deposits in the world. It has extraordinarily well preserved primary geochemical and sedimentary features. As such, the HYC is ideally suited for elucidating the role of organic matter and ore fluid interactions in this important class of ore deposits.

Despite detailed studies interpretations of the genesis of the ore vary widely. Currently, there are two principal models proposed for the formation of the McArthur River deposit; (1) a predominantly exhalative (sedex) process producing mineralisation at the sediment surface [1–5], (2) an early diagenetic ("epigenetic") process occurring at shallow subsurface depths [6,7]. In addition, two environmental models have been proposed. The first, shallow water lacustrine and/or a sabkha environment [8–11], is based on the interpretation of nodular dolomite textures within and around the orebody. The second, deep-water marine setting, is based on sedimentological and geochemical interpretations [3,5,12,13].

Previous organic geochemical studies recorded all organic maturity indicators from host rocks to correspond to thermal maturities within the oil window. However, samples taken from within the ore zones show slightly higher maturities in response to ore processes. These studies [e.g. [14,15]]

concentrated on sampling the ore and its associated sediments on a centimetre to millimetre scale within a single orebody (2 orebody) exposed within the mine [14]. Hydrocarbon biomarker distributions in ores collected from 2 orebody have revealed a series of C_{26} to C_{30} steranes derived from a marine Chrysophyte algae [14]. This signature implies that the organic matter in the Barney Creek Formation had a marine source. More recently, [15] analysed polycyclic aromatic hydrocarbons (PAHs) in two orebody and noted that the PAH compound distribution patterns are similar to those of hydrothermally-generated petroleum in the Guaymas Basin, Gulf of California, and Middle Valley, Juan de Fuca Ridge, [16–21]. Moreover, this PAH compound distribution is significantly different from those found in conventional petroleum accumulations. Furthermore, PAH abundances and isomer distributions were shown to reflect a temperature gradient between the source of mineralising fluids and the sediments fringing the ore system during ore formation. High molecular weight PAH's, such as coronene, were found to be most abundant close to zones of highest temperature and decrease in abundance away from these hot zones. The fluid pathway is not well understood; [15] propose a carbonate disolution mechanism to provide a fluid pathway. An alternative model is that the fluid pulsed through the sedimentary sequences in a batch wise mechanism [22]. The fluid pathways of each pulse being further controlled by depth and temperature.

In general, the ore-forming fluid is considered to have been moderately hot (100–250 °C), oxidized (sulfate > sulfide) brine, which was rich in sulfate and metals, at the point where it entered the basin [3,4,6,8]. Based on the presence of higher molecular weight PAHs higher initial fluid temperatures in the range of 250–400 °C have been suggested at the source of the fluid [15].

The aim of this current study is twofold, firstly, to investigate ore fluid interaction with the insoluble kerogen component and assess any impact of burial on the kerogen molecular structure. Secondly, to determine if the mobile bitumen in the regional sediments has any preserved signals pertaining to the ore formation processes.

Solid state techniques such as laser Raman spectroscopy, X-ray photoelectron spectroscopy (XPS), Fourier transform infrared spectroscopy (FTIR) and chromatographic techniques have been combined to elucidate the structure of the kerogen and molecular composition of the bitumen from the HYC ores and host rocks.

Samples were collected laterally and vertically through the successions outside the mine (Fig. 1) to assess hydrothermal and diagenetic processes affecting the McArthur River ore deposit on a broader regional setting. The results are compared to modern hydrothermal systems where signals from the interaction between hot fluids and organic matter have been recognised for example [17–22].

2 Geological Setting

The McArthur Basin is a 200,000 km^2 area of unmetamorphosed and relatively undeformed Palaeoproterozoic sediments in the Northern Territory, Australia (Fig. 1). The succession is divided from bottom to top into the Tawallah Group, McArthur Group, Nathan Group, and the Roper Group. The McArthur Group is a succession of interbedded dolostone, red beds and quartz arenite, sedimentary breccia, siltstone, and tuff. The McArthur River Pb–Zn–Ag deposit is hosted near the base of the HYC Pyritic Shale Member of the Barney Creek Formation within the McArthur Group.

The host sediments of the ore are dark carbonaceous and pyritic dolomitic graded siltstones and mudstones with abundant graded breccias of pre-Barney Creek dolomite [23,24] interbedded with sedimentary mass flow units [9]. The breccias, as described by [24] contain a wide variety of clast sizes ranging from gravel size to tens of meters in diameter. Clast composition is described to vary considerably, although most are of a dolomitic nature. Some sulphidic clasts, similar to the in-situ mineralized facies are present, thus clast compositions suggest a range of sources. The siltstones have parallel laminae 0.5–50 mm thick, locally, with small scale cross lamination, scour and fill, graded textures and slumping [3,4,23–25].

Two transgressive/regressive cycles, are reported in the HYC sub-basin [13]. These, and other sediment transport mechanisms may have been tectonically controlled [9,16].

Mineralisation consists mostly of pyrite, sphalerite and galena in varying proportions, finely disseminated throughout the siltstone. Ore-rich laminae are often enclosed between layers of poorly mineralised to unmineralised mudstone and siltstone. Sulfide concentrations within ore laminae are commonly greater than 60% by weight [8,23]. Unmineralised layers are present throughout the succession and vary in thickness from millimetre-scale mudstone layers, centimetre-scale turbidites to metre scale breccia beds.

Isotopic analysis and detailed study of the mineral textures have shown that the orebody contains several phases of sulfide [6,26]. They suggested an early diagenetic pyrite phase (Py 1) which was generally followed by a later and slightly coarser grained pyrite phase (Py 2) and this, in turn was over-printed by sphalerite and galena. Py 1 has a ∂^{34} S values consistent with the formation by bacterial sulfate reduction (BSR) in a system open to sulfate, and probably formed at, or close to, the sediment-water interface, possibly incorporated into the sedimentary pile via pelagic fall out [6]. Py 2 is enriched in ∂^{34} S relative to coexisting py 1. This has been explained as resulting from later "closed-/partially closed" system reduction within the sediment pile [6,26,27] or by the incorporation, within the BSR pyrite zone immediately beneath the sediment-water interface, of excess heavy

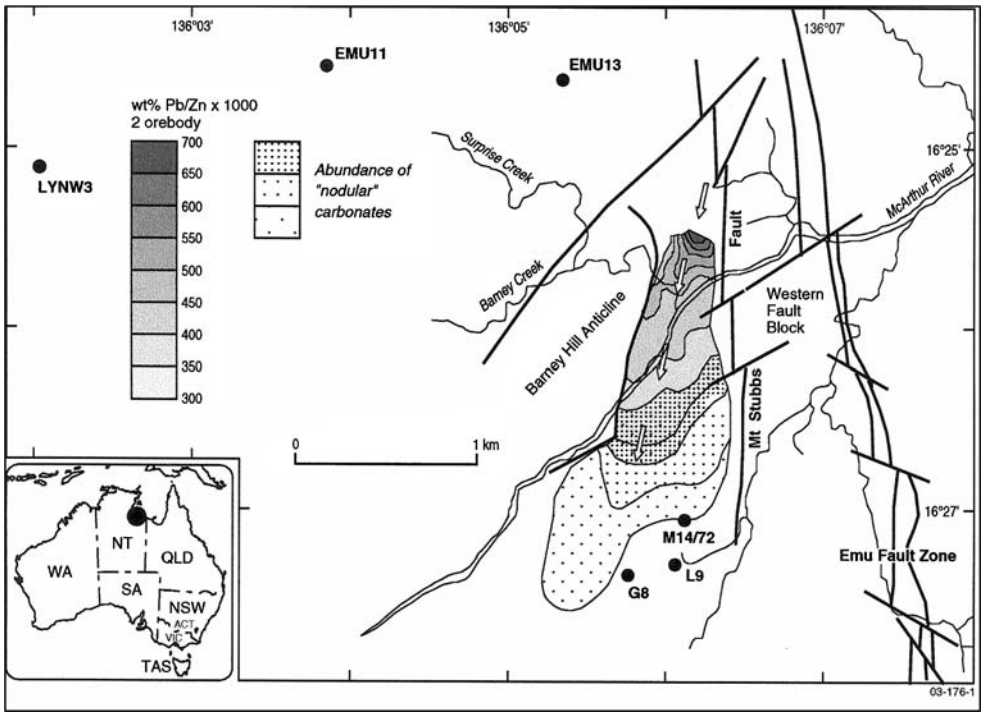

Fig. 1 Map of the McArthur River mine and surrounding region showing sample locations and metal ratios. Hypothesized flow of the mineralizing brine is indicated by arrows

sulfate in the out-flow zone of the sub-surface mineralizing system [8]. Based on SHRIMP measurements, ∂^{34} S values for galena and sphalerite range between −5 and +5 $^{0}/_{00}$. This mineralization is thought to involve reaction of sulfate in the hydrothermal ore solution with organic matter within the Barney Creek Formation [8,28,29]. [6] Suggest a dis-equilibrium between sphalerite and pyrite phases. A rapid formation mechanism, with a constant replenishment of the brine pool by diffusion across the brine-anoxic boundary zone could explain the low variability in sulfide isotopic signatures for sp1. In contrast, the wide variability in sulfur isotopic signatures for py1 may reflect the multiple sources of aqueous sulfide utilised during py1 formation with subsequent phases of sphalerite and pyrite being generated by diagenetic processes.

3 Sampling

To assess hydrothermal and diagenetic processes affecting the McArthur River ore deposit on a regional setting, samples were collected laterally and vertically through the various geological successions outside the mine (Fig. 1). Analytical results are compared to modern hydrothermal systems where signals from the interaction between hot fluids and organic matter have been recognised in the literature for example [17–22].

4 Experimental

4.1 Kerogen isolation

The isolation of kerogen was conducted by Loala Pty Ltd, Bellevue, Western Australia following the standard Hydrofluoric acid/ Hydrochloric acid (HF/ HCl) kerogen extraction procedure [30]. The kerogens were isolated from portions of pulverized and homogenized samples after bitumen extraction (see below).

4.2 Bitumen extraction

The surface of the rock samples was cleaned with CH_2Cl_2 to remove possible contamination during sample collecting. Rock samples were ground to <200 mesh grain size and extracted using the automated Dionex ASE 200 following the method of [31] (100 % CH_2Cl_2 at 100 °C, 1,000 psi, preheat 2 min, heat 5 min, static 2 min, flush 120%, purge 120%, cycles 5). Extracted Organic Matter (EOM), bitumen, was reduced to approximately 3 mL by thermal rotary evaporation. This was further reduced by 50% under a steady stream

of nitrogen. At this stage elemental sulfur was removed using activated copper short columns.

4.3 X-ray photoelectron spectroscopy (XPS)

The XPS spectra of the kerogens were recorded on a VG ESCALAB 220i XL spectrometer with a hemispherical electron analyzer and a monochromatic Al source operated at 10 kV and 20 mA with a base pressure of approximately 5×10^{-8} torr. Powder samples were finely ground and spread by mounting evenly across sample stubs (to create a uniform level of sample charging) using double sided adhesive tape. The X-ray beam was focused onto the kerogen samples using an X-ray spot size of $150 \times 800\,\mu m$ in order to exclude substrate from the analysis. A small area XL 150 μm lens was used. The insulating nature of kerogen results in surface charging, which is observed as a shift to higher binding energy of all peaks in the X-ray photoelectron spectra. Differential charging occurs when different species in a heterogeneous surface, such as organic and inorganic species in kerogen, electrostatically charge by different amounts. Thus to compensate for sample charging a magnetic lens and electron flood source was used during spectral acquisition. Spectra were charge corrected by assigning a value of 285.0 eV to the principal carbon 1 s photoelectron peak component, corresponding to aromatic and aliphatic C–C and C–H species.

Wide scan spectra, covering the binding energy range of 0–1100 eV was initially recorded to give elemental composition of the kerogen. Wide scan spectra were collected with pass energy of 100 eV and a step size of 1 eV with 3 scans. Structural information was obtained by elemental region scanning of core-level signals from C 1 s, N 1 s, O 1 s, and S 2 p. Region scans were collected with a pass energy of 20 eV with a step size of 100 meV ranging from 5 to 30 scans depending upon elemental concentration. The binding energy scale was calibrated to the Cu $2p_{3/2}$ ($E_B = 932.7$ eV) and Au $4f_{7/2}$ ($E_B = 84.0$ eV) lines.

The C 1s, N 1s, and S 2p photoelectron peaks were deconvoluted with a Gaussian/Lorentzian fit routine used within the Eclipse V2.0 software. Linear background subtraction and Gaussian peak deconvolution were performed by the root mean square (r.m.s.) goodness-of-fit to the measured peak shape. This was constrained as unity or less, and the full-width at half-maximum (FWHM) of the synthetic Gaussian peaks was constrained to lie between 1.0 and 2.5 eV. The S 2p spectra were complicated therefore, the spectra were fitted using doublets of S 2p1 and S 2p3 (intensity ratio 1:2 and BE differences of 1.18 eV). The number of electrons counted having a specific energy, (which is directly related to the surface concentration of the elements analysed), is expressed as percentage atomic concentration (AT%). The atomic concentrations (AT%) of various elements present were calculated from the measured peak areas using Eclipse V2.0 software with the following sensitivity factors: Zn, 18.92; Cu, 16.73; Fe, 10.82; O, 2.93; N, 1.80; C, 1.00; S, 1.11.

4.4 Raman spectroscopy

The Raman spectra were acquired on a Renishaw Raman Microprobe Laser Raman Spectrometer using a charge coupled detector. The collection optics are based on a Leica DMLM microscope. A refractive glass 50× objective lens was used to focus the laser onto a 2μm spot to collect the backscattered radiation. The 514.5 nm line of a 5W Ar^+ laser (Spectra-Physics Stabilite 2017 laser) was used to excite the sample. Surface laser powers of 1.0–1.5 mW were used because kerogens were found to burn under higher energies. An accumulation time of 30 s and 10 scans were used which gave adequate signal-to-noise ratios of the spectra. The scan ranges were in the carbon first-order region from 1,000 to 1,800 cm^{-1}. Kerogen samples were deposited on clean aluminum microscope slides and irradiated with the laser to obtain spectra. The operating conditions of the laser Raman spectrometer were optimised by focussing the laser (20 mW power) onto a film of silicon and adjusting the alignment of the laser to obtain the greatest possible signal at approximately 520 cm^{-1} with an accumulation time of 1s.

Spectral manipulation such as baseline adjustment, normalization and full-width at half-maximum was performed using the GRAMS32 software package (Galactic Industries, Salem, NH, USA). The full-width at half-maximum (FWHM) of the graphite (G) band was determined by drawing a line parallel that intersects the middle of a vertical line connecting the maximum (or minimum) of the band and the local baseline. The distance between both intersection points of this parallel and the spectrum is the half-line-width.

4.5 Gas chromatography/mass spectrometry (GC/MS)

Full scan and selective ion recording (SIR) GC-MS analyses were performed on a HP5973 Mass Selective Detector (MSD) instrument equipped with a HP6890 GC using split-splitless 7683 Series injector (Hewlett Packard) in splitless mode with a 60 m × 0.25mm i.d. fused silica tubular column coated with 0.25μm DB-5 stationary phase (J&W Scientific) and helium (He) carrier gas. For full scan analyses of the extracted organic matter (EOM) and aromatic fraction the GC was programmed from 40 °C for 2 min, followed by a temperature ramp of 4 °C/ min, and an isothermal period of 20 min at 310 °C. All mass spectral data were obtained with an ionisation energy of 70 eV over the mass range 50–550 Da with a scan rate of 3 scans/s. For SIR analyses of saturate fractions the GC was programmed from 40 °C for 1min, followed by a temperature ramp of 10 °C/min to 150 °C, then 2 °C/min to 310 °C.

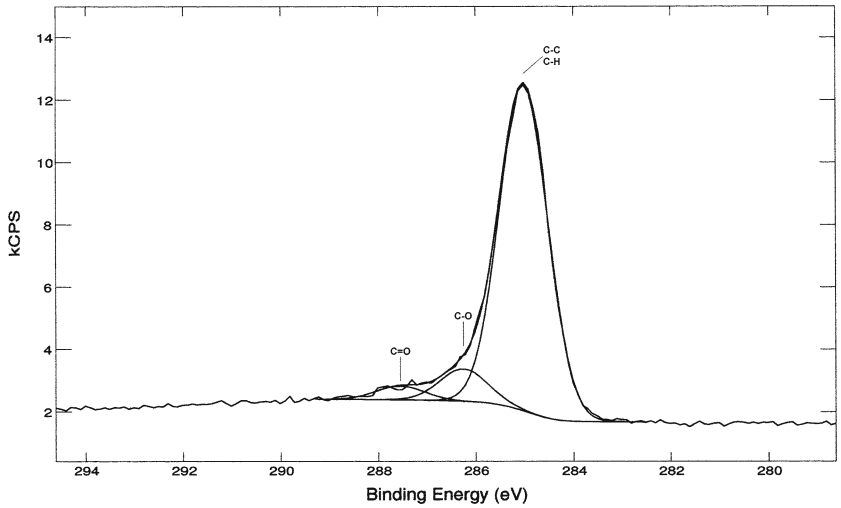

Fig. 2 C 1 s photoelectron spectrum of kerogen from the hot zone of two orebody showing deconvoluted Gaussian–Lorentzian components

Saturates were identified by GC-MS in SIR mode, aromatics were identified by GC-MS in full scan mode for both, comparison of retention times were made with AGSO II standard. Adamantanes and diamantanes were identified by GC-MS in full scan mode and compared with mass spectra and chromatographic data presented in [32]. Diamondoid adamantanes were monitored by ions at *m/z* 136 (adamantane), 135 (methyl adamantanes), 188 (diamantane) and 187 (methyl diamantanes). 50 ng d14-terphenylwas used as the internal standard for quantitative purpose. The relative response factors of d14 to other compounds, including phenanthrene, 9-me-phenanthrene, fluorene, dibenzothiophene (DBT), and nC_{19} have been calculated.

5 Results

5.1 Kerogen samples from the region

Structural information can be derived from the line-shape analysis (deconvolution) of the individual core-level signals of XPS spectra. Line-shape analysis was performed on carbon, nitrogen and sulphur core-level signals. The C 1s core-level photoelectron peak can be resolved by deconvolution into three Gaussian–Lorentian components for the eight kerogen samples from orebody two and four Gaussian–Lorentian components for the samples outside the orebody. The major component of the C 1 s envelope at 285 eV binding energy is assigned to non-functionalised aromatic and aliphatic carbon hydrocarbons (C–C and C–H). Minor components at 285.9 and 287.1 eV are assigned to carbon bonded to oxygen (C–O and C=O, respectively) (Fig. 2). Samples from outside the orebody have C 1 s spectra with an additional component at 288.6 eV assigned to carbon bound to two oxygens (COOH) [not shown].

The ratio of carbon and hydrocarbon/carbon-oxygen groups indicate that outside the orebody the kerogen contains the least amount of carbon-oxygen functional groups and therefore, is less thermally mature. The kerogen from the host sediments recorded little variation between the quantities of carbon-oxygen functional groups.

For an ideal graphitic crystal (space group D^4_{6h} with unlimited translational symmetry) only one first-order band, the G (graphite) band is exhibited at 1,580 cm^{-1} corresponding to an ideal graphitic lattice vibrational mode with E_{2g2} symmetry [33]. It has been assigned as a C–C stretching in the longitudinal symmetry axis of the graphite plan. Disordered carbonaceous materials, as shown by the representative curve-fitted spectra of isolated kerogen from the SPC (Fig. 3), on the other hand, exhibit additional first-order bands (D or Defect bands), which are known to be characteristic of disordered sp^2 carbons and increase in intensity relative to the G band with further disorder introduced into the carbonaceous network.

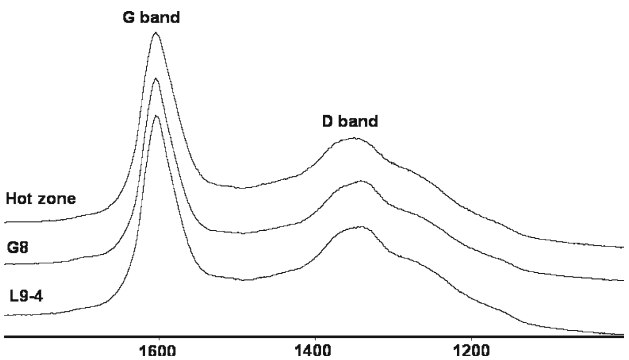

Fig. 3 Representative first-order laser Raman spectra of kerogen samples from the hot zone of two orebody (HOT zone), G8 drill core sample (G8), and L9-4 drill core sample (L9-4)

Four D bands are visible (Fig. 3). The most intense of the D bands is that appearing at ~1,350 cm^{-1}. This band corresponds to a disordered carbon lattice vibration mode with A_{1g} symmetry; a mode suggested to arise from graphene layer carbon atoms in immediate vicinity of a lattice disturbance such as the edge of a graphene layer [34,35] or a heteroatom [35]. The D band displays a poorly defined shoulder at ~1,285–1,295 cm^{-1}. The origin of this shoulder has two possible assignments; firstly one proposed by [36] who assigned this shoulder to a diamond-like atomic arrangement, that is, sp^3 hybrised carbon. The second assignment proposed by [37] is that the shoulder represents broadening due to a combination of highly condensed aromatic hydrocarbon compounds. In our case, the second interpretation is the most likely due to the highly aromatic bitumen extracted from sediments of the study area. Another first-order band pertaining to structural disorder is the D band at ~1,620 cm^{-1} which can be observed as a shoulder on the G band. This shoulder becomes further developed in more disordered carbonaceous materials. The G and D bands merge, until a single feature is observed around 1,600 cm^{-1}. This feature produces an apparent band broadening and up-shifting of the G band. The D band at ~1,620 cm^{-1} corresponds to a graphitic lattice mode with E_{2g} symmetry [35] and is assigned to a lattice vibration involving graphene layers at the surface of a graphite crystal [35]. The relative intensities of both the D band at ~1,350 cm^{-1} and the D band at ~1,620 cm^{-1} increase with increasing excitation wavelength, which can be attributed to resonance effects [38]. The high signal intensity between the G and D band maxima can be attributed to the additional band seen at ~1,550 cm^{-1}, which has been assigned to amorphous carbon fractions of organic molecules, fragments or functional groups [39,40]. In pure amorphous carbon materials this band at ~1,550 cm^{-1} becomes the dominant broad intense feature of the carbon first-order spectrum. The D band at ~1,350 cm^{-1}, exhibits a shoulder at ~1,200 cm^{-1} (Fig. 3). This shoulder has been tentatively attributed to $sp^2 - sp^3$ bonds or C–C and C=C stretching vibrations of polyene-like structures. These polyene C–C=C–C structures are bridging units that link the aromatic domains.

The width and relative intensities of D and G lines vary with structural evolution and may be used to characterise carbon materials. The ratio of band intensities $I_D/(I_D + I_G)$, expressed as a percentage, is most frequently used as a disorder parameter. G band FWHM is also used, particularly in assessing the thermal maturity of coals and kerogens.

$I_D/(I_D + I_G)$ ratios for a representative set of kerogen samples from drill cores and mine sites (Table 1) show that the kerogen from the hot zone of orebody two has the higher degree of structural disorder. Kerogen in the cooler zones has the least structural disorder. Outside the orebody the trend is not so simple with varying order described across the regional area.

Table 1 Raman spectroscopic parameters derived from kerogen analysis

Sample locality	G FWHM (cm^{-1})	$I_D/(I_D + I_G)$
Emu 11	52.7	35.03
Emu 13	48.9	36.18
LW 3	57.5	35.73
Hot zone	52.6	34.72
Cool zone	50.7	5.44
M14	57.4	35.32
L9	48.6	35.17
G8	61.2	36.03

The G band FWHM is a good indicator of thermal maturity, particularly for aromatic kerogens. The Raman carbon first-order spectra display a line-shape that suggests an anthracite-like structure, yet the G band FWHM indicates a much lower rank (Fig. 3). This disparity between the data may be a function of Proterozoic kerogen structure. The data suggest that Proterozoic kerogen has a higher aromaticity and ordering throughout a polycondensed network which could conceivably produce a false thermal signal. Palaeoproterozic organic matter has a microbial source [14], but it seems that many Proterozoic kerogens with a relatively mild thermal history are more similar to aromatic-rich kerogen type III rather than the aliphatic-rich kerogen type I this may lead to mis-interpretation of the maturity of samples analysed. The aromaticity could be a function of Proterozoic organic matter resulting in highly aromatic recalcitrant components that have cross-linked during early maturation and diagenesis or selectively preserved in kerogen formation.

In our study, G band FWHM was used to elucidate any burial trends in the surrounding region of the orebody. The assumption being that deeper samples are hotter and therefore expected to be more structurally ordered, burial would therefore lead to a trend towards a reduced G band FWHM. Burial trends were only observed in three of the six drill holes examined. G8 showed the most notable trend with a reduction in G band FWHM from 61.2 to 54.9 cm^{-1} over 138.6 m change in depth (Fig. 4).

Previous studies of G band reduction of Raman spectra of coals and kerogens [41] have observed that the G band FWHM can be correlated to vitrinite reflectance (Ro%). With a G band reduction of 61.2–48.6 cm^{-1} recorded in our study we can assume a Ro% range from 1.3 to 2.0%. According to [42] this Ro% correlates to a palaeotemperature of ~120–180 °C.

In general the overall macromolecular structure and composition of the kerogen isolated from 2 and 8 orebodies, and

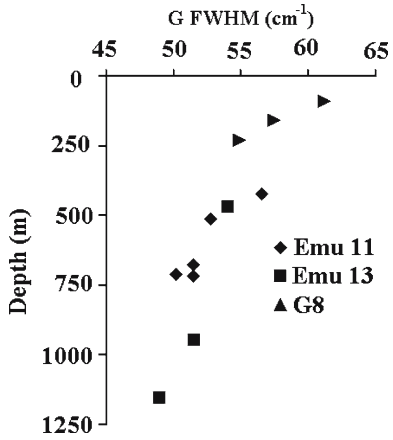

Fig. 4 Depth profiles of the G band FWHM of kerogen samples from Emu 11, Emu 13, and G8 drill core samples

the host Barney Creek Formation are similar; however differences in functional group abundance show that 2 orebody has experienced higher temperatures. Nevertheless, the molecular structure is consistent with the kerogen throughout the region undergoing late stage catagenesis, indicating a regional thermal overprinting event with temperatures not rising above 180 °C.

5.2 Bitumen from 2 orebody

Studies of active hydrothermal systems where organic matter and mineralising fluids interact for example, [16–21] can be used as a window into similar processes operating in ancient sediments. These studies of active hydrothermal systems have shown that hot fluids passing through organic-rich mud can generate oil (bitumen) and gas. These bitumens contain characteristic patterns of PAHs with low levels of alkylation and increased abundances of large, multi-ring members such as benzopyrene, benzoperylene, and coronene [15,43,44]. In the Guaymas Basin, vented fluids containing hydrothermally generated PAHs have temperatures greater than 300 °C. The rapid heating rates developed during the interaction of hot brines and organic matter are thought to favour the formation of non-alkylated and highly condensed PAHs. In addition, elevated abundances of PAHs have also been observed in ancient mineral systems such as Red Dog Pb–Zn mine, North West Alaska [45] and Kupferschiefer Shale (Cu–Pb–Zn) in Europe [46,47]. In modern systems such as the Guaymas Basin, the hydrothermally generated petroleum condenses in conduits and vugs as the temperature decreases. PAHs precipitate near the hotter vent chimneys with the metals, the waxes are precipitated at intermediate temperatures (20–80 °C), and heavy oil accumulates in the cooler regions [48].

Within two orebody the bitumens exhibit two compositional end members based on total ion chromatograms (TICs) acquired during full-scan GC/MS analysis of the extracted bitumens (Fig. 5).

Bitumens from the northern hottest areas of two orebody are dominated by aromatic hydrocarbons, and in the cooler southern area they are dominated by aliphatic hydrocarbons. Within two orebody, the signal grades between these end members from the hottest to the coolest zones. In the hot zone of two orebody both ore and enclosing mudstone lithologies are dominated by aromatic hydrocarbons.

Bitumen from drill holes G8 and M14, which are located on the southern fringe of two orebody (Fig. 1), show a relative

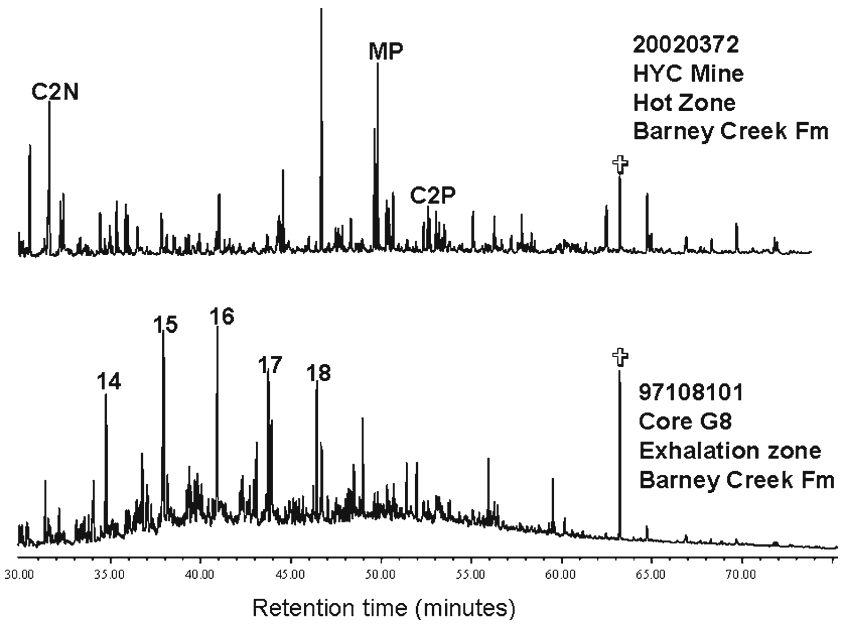

Fig. 5 Plot of TIC acquired from 1/4 aliquots of the extracted organic matter (EOM) obtained from the bitumens of the hot and cool zones of two orebody highlighting the two end members, exhalative zone, aliphatic dominated and hot zone aromatic dominated. The general elution order of aromatics is denoted as $C2N$ = C2 napthalenes, $C2P$ = C2 phenanthrenes, MP = methyl phenanthrene, and †= internal standard, for the aliphatic dominated member the carbon numbers of the major alkane homologues are provided

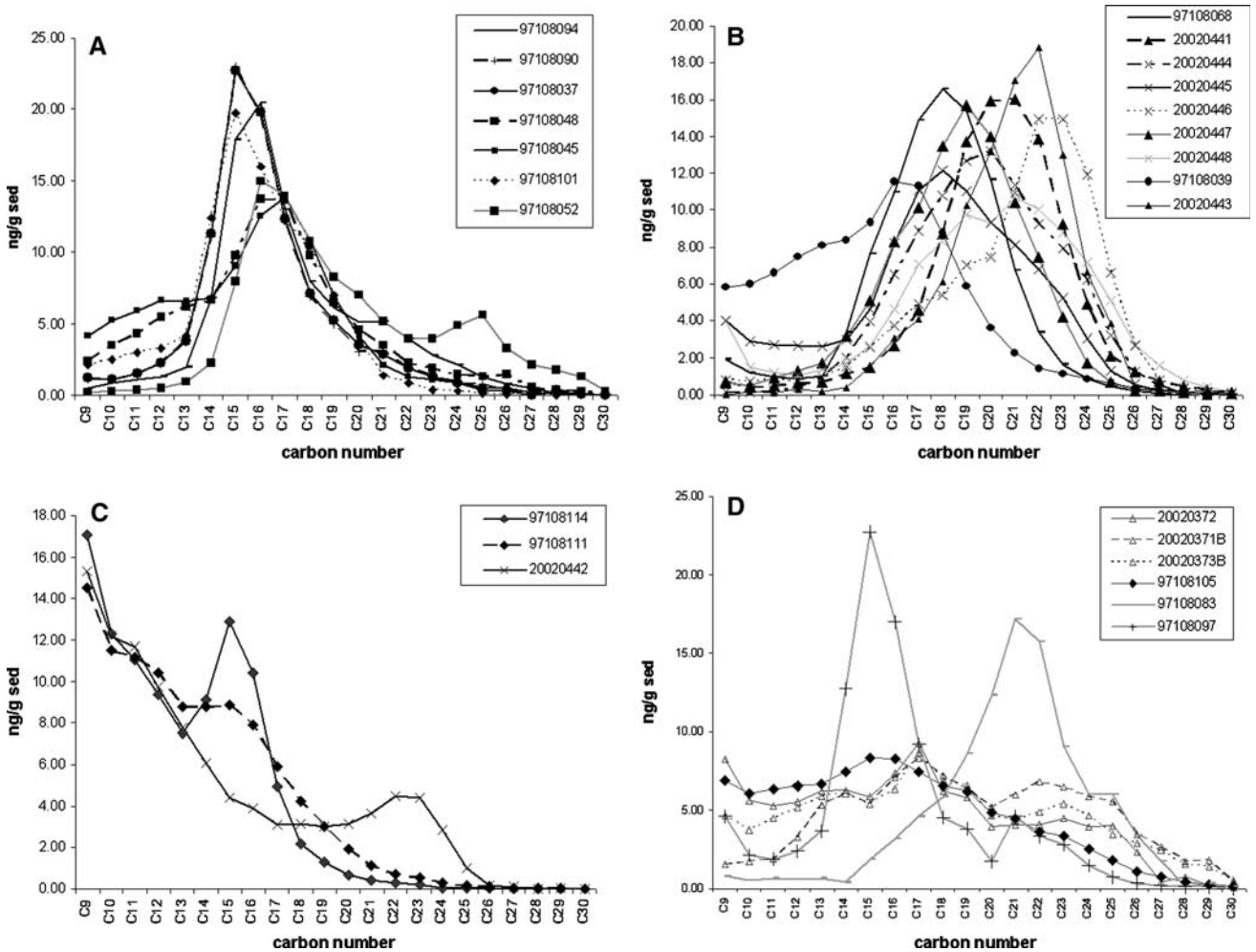

Fig. 6 Plot of *n*-alkane distribution within the bitumen where four distribution patterns were recorded. The various cores and mine samples analysed are represented by the following symbols: *Filled bar* L9, *Filled triangle* E13, *Filled diamond* G8, *Filled Circle* LW3, *Plus symbol* M14, *Multi symbol* E11, and *Open triangle* Handspecimens

increase in the aliphatic hydrocarbon signal. This observation is consistent with hydrothermally generated petroleum precipitating higher molecular weight aromatic hydrocarbons in hotter regions, while the lower molecular weight aliphatic hydrocarbons accumulate in the cooler and the fringing zones of the ore system along the palaeo-flow pathway.

5.3 Regional organic geochemistry

Aromatic and aliphatic hydrocarbon signals were examined in regional samples to determine the extent of hydrothermal activity and palaeo-environmental settings. In general, the further away from two orebody, the greater the predominance of aliphatic hydrocarbon signals. As outlined above, this signal is interpreted as evidence of hydrothermal petroleum generation.

Four *n*-alkane distributions are observed in samples taken from the Barney Creek Formation (Fig. 6). A narrow distribution is observed in cores fringing the ore deposit (M14, L9, and G8). This narrow distribution ranges between $n\mathrm{C}_{13}$ and $n\mathrm{C}_{19,}$ with a maximum at $n\mathrm{C}_{15-16}$ (Fig. 6a).

A broad *n*-alkane distribution is also observed, in samples fringing the deposit, and samples obtained from several kilometers away (Emu 11 and Emu 13). The broad distribution ranges between $n\mathrm{C}_{14}$ and nC_{26}, with a maximum between $n\mathrm{C}_{17-21}$ (Fig. 6b).

If we compare this signal with that described in the ore itself, the signal is much narrower outside the mine. Within the mineralised zones of two orebody, a very broad distribution of *n*-alkanes ranging from nC_{10} to $n\mathrm{C}_{28}$ with no distinct maxima is observed. This pattern is clearly different from the previously described *n*-alkane distributions (Fig. 6d).

A fourth distribution of *n*-alkanes is characterized by increasing concentrations of lower molecular weight components, maximising around nC_9 (the first *n*-alkane to be

quantified, Fig. 6c). This pattern appears to overprint the broad or narrow distribution described above.

These overprinted samples are interpreted to be oil stained, with the higher molecular weight *n*-alkanes representing the in situ bitumen derived from normal burial maturation of the samples. The oil stains occur in two samples from G8, close to the mine. As hydrothermal petroleum migrates and cools, precipitation occurs along the flow pathway. High molecular weight PAHs drop out of solution before lower molecular weight components and hydrocarbons travel further along the flow pathway. These oil stained samples may represent evidence of migrated hydrothermal petroleum on the fringes of the outflow.

The *n*-alkane patterns show no strong facies signal and no significant maturity differences. The pattern shown by the *n*-alkane suggests a mixing of hydrothermally generated oil with shorter chain length hydrocarbons overprinting bitumen derived from natural burial maturation, characterised by longer chain length hydrocarbons.

5.4 Organic matter source

Biomarker concentrations were unfortunately too low in the extracts to make reliable interpretations of source variation. However, ratios of dibenzothiophene (DBT)/phenanthrene against pristane/phytane have previously been used to assess environments of deposition [49]. In this study DBT concentrations are low relative to most aromatic components (Table 2). This is often interpreted to indicate that the environment was sulfur poor. However, in these sediments the low organic sulfur incorporation can easily be explained by the high metal concentrations within the Barney Creek Formation. Therefore, the low DBT/phenanthrene ratio is directly influenced by the abundance of metal ions during sulfide formation. Furthermore, throughout the Barney Creek Formation, pristane to phytane ratios are low, and range from 0.3 to 1.9 (Table 2). This is typical of Proterozoic material, which has a high bacterial and algal input. These findings support the lacustrine to marine lacustrine anoxic environment

Table 2 Ratios and maturity indices used in interpretation and analysis

Sample number	Well name	Depth (m)	Formation	Pr/Ph	Pr/C17	Pr/C18	MPI	DBT/P	MDI	MAI
20020372	Mine	–	BC	0.40	0.10	0.50	1.17	0.02	0.452	0.866
20020371B	Mine	–	BC	0.60	0.20	0.40	1.17	0.03	0.443	0.886
20020373B	Mine	–	BC	0.50	0.20	0.40	1.21	0.02	0.463	0.892
97108097	L9	508.8	BC	1.50	0.70	1.00	1.14	0.08	0.461	0.872
97108094	L9	554.8	BC	1.50	0.50	0.60	1.04	0.08	0.447	0.868
97108068	M14	261.6	BC	1.10	0.30	0.20	1.30	0.14	0.378	0.735
97108083	M14	410.8	BC	0.80	0.40	0.40	1.01	0.07	0.430	0.841
97108090	M14	466.2	BC	1.50	0.60	0.80	0.81	0.07	0.455	0.884
97108114	G8	91.1	BC	1.90	0.40	0.40	1.28	0.04	0.343	0.652
97108101	G8	157.1	BC	1.10	0.50	0.60	1.15	0.11	0.394	0.693
97108111	G8	195.5	BC	1.20	0.40	0.40	1.17	0.13	0.370	0.738
97108105	G8	229.7	BC	0.80	0.20	0.30	1.43	0.05	0.390	0.744
97108052	LW3	188.0	Reward	0.80	0.70	1.00	0.93	0.43	0.375	0.476
97108048	LW3	233.4	Reward	0.90	0.40	0.70	0.95	0.37	0.072	0.643
97108045	LW3	282.6	Reward	0.90	0.30	0.40	0.95	0.41	0.188	0.610
97108039	LW3	324.9	BC	0.90	0.20	0.30	0.87	0.24	0.142	0.613
97108037	LW3	337.3	BC	1.20	0.60	1.00	0.81	0.08	0.460	0.870
20020447	Emu 13	467.7	BC	0.90	0.20	0.10	1.11	0.06	0.532	0.936
20020441	Emu 13	947.0	BC	0.40	0.20	0.20	1.25	0.05	0.676	0.931
20020443	Emu 13	1153.0	BC	0.30	0.00	0.00	0.88	0.05	0.708	0.990
20020442	Emu 11	422.4	BC	1.40	0.30	0.20	1.34	0.04	0.346	0.677
20020445	Emu 11	511.0	BC	1.50	0.40	0.20	1.41	0.08	0.364	0.682
20020446	Emu 11	675.3	BC	1.00	0.30	0.30	1.21	0.04	0.422	0.843
20020448	Emu 11	710.4	BC	0.60	0.10	0.20	1.21	0.03	0.441	0.846
20020444	Emu 11	715.3	BC	0.90	0.10	0.10	1.15	0.08	0.431	0.846

Pr = pristane, *Ph* = phytane, *C17* = C_{17} *n*-alkane, *C18* = C_{18} *n*-alkane, *P* = phenathrene, *MP* = methyl phenathrene, *MPI* = methyl phenanthrene index, *DBT* = dibenzothiophene, *MDBT* = methyldibenzothiophene, *BC* = barney creek formation, and *Reward* = reward formation

implied by DBT/phenatherene against pristine/phytane ratios [49].

5.5 Bitumen maturity trends

Bitumen within the ore deposit and host sediment is a mixture of hydrothermal petroleum overprinting bitumen produced from the in situ organic matter during burial. For this reason the assessment of maturity parameters is complicated and typical maturity trends are not observed down core in samples fringing the mine. Nevertheless, Methyl Phenanthrene Indices (MPI), [50] do show a slight trend, values between 1.01 and 1.43 from the ore bearing samples, and 1.14–1.21 in the mudstone samples within two orebody, and 0.87–1.41 in Barney Creek Formation were observed (Table 2). Generally, the highest values are observed within the ore and lower values are observed outside of the deposit (Table 2).

Diamondoid maturity parameters [31] give Methyl Diamantane Indices (MDI) ranges of 0.34–0.67 and Methyl Adamantane Indices (MAI) values of 0.47–0.93. This correlates with R_o maturity levels of 1.1–1.6% [42,51] and is consistent with G Band FWHM maturity assessments outlined previously.

6 Conclusions

The kerogen from orebody two and the surrounding region are characterised by a highly condensed polyaromatic network and show little to no variation in burial parameters. However, subtle trends can be delineated within two orebody and the surrounding sediments. Increasing carbon-oxygen functional group content is observed from kerogen samples in the hotter parts of the ore zone grading into the cooler areas. The ratio of carbon and hydrocarbon/carbon-oxygen groups clearly indicates that outside the orebody the kerogen is less thermally mature.

Within two orebody, two end members can be delineated by GC/MS analysis of the extracted bitumen. Bitumens from the northern hottest areas of two orebody are dominated by aromatic hydrocarbons, and in the cooler southern area they are dominated by aliphatic hydrocarbons. Within two orebody, the signal grades between these end members from the hottest to the coolest zones. This observation is consistent with hydrothermally generated petroleum precipitating higher molecular weight aromatic hydrocarbons in hotter regions, while the lower molecular weight aliphatic hydrocarbons accumulate in the cooler fringing zones of the ore system along the palaeo-flow pathway (down gradient). In general, the further away from two orebody, the greater the predominance of aliphatic hydrocarbons.

Thermal cracking of aliphatic components may have occurred during the hydrothermal activity, this may inturn have led to the generation of low molecular weight n-alkanes, imparting the narrow, low molecular weight distribution described in this study.

Vitrinite reflectance, Ro% values defined by both kerogen and bitumen analysis concur; the final thermal maturity of the organic matter of two orebody lies within the zone corresponding to wet gas generation, with a maximum burial temperature range of 120–180 °C. This in-situ burial process is the most likely source of the oil staining seen in several of the samples analysed across the fringes of the mine.

The lack of evidence of HMW PAH indicates that the higher temperature suggested by [15] for ore formation at the HYC may have been highly localised. Interpretation of the data reported in this study can support the assertion that hydrothermally derived fluids extended into the host sediments, however, we suggest that it is likely that fluids were much cooler by this point.

The dynamic nature of the sedimentary environment in which the orebodies formed preclude the delineation of a fluid flow pathway extending into the regional area. The previously identified complex sedimentary processes including; transgressive/regressive cycles in the deepest water environments, potentially leading to substantial reworking of the syn-sedimentary organic matter; hydrothermal and thermochemical organic matter synthesis, with concomitant acid catalysis of the organic matter resulting in changes in ionic strength of the mineralizing fluid; and similarity of the breccia clast composition to the in-situ mineralization, make interpretations difficult. Nevertheless, we can conclude that the geochemistry of the host sediments of the HYC deposit has been influenced by physical, chemical and biological processes. The resulting chemical signatures reflect a mixture of organic matter sources ranging from shallow enclosed/partially closed possibly lacustrine environments, to a deep marine environment below wave base. Furthermore, our evidence supports a model allowing in-situ alteration of the deposited organic matter through hydrothermal and diagenetic processes.

Acknowledgments This paper represents the views of the authors and may not be representative of the views of Geoscience Australia where the analysis was carried out. The authors would like to thank Dr Graham Logan and Dr Junghong Chen for their advice on the sampling of the sediments and discussions of their previous analytical work. Dr Paul Greenwood is thanked for his expert help and advice on GC-MS and Py-GC-MS analysis. Janet Hope and Rachel Davenport are thanked for their technical advice and support. Karen Mackenzie would like to thank Neil Williams for his enthusiastic discussions regarding the geology of the HYC deposit and McArthur River area. Brian Pashley is thanked for his preparation of the HYC deposit figures.

We thank the McArthur River Mining Company for access to the mine and MIM Exploration for permission to sample core material, and particularly Mr Steve Pevelly for a map of the drill hole and mine site. Karen Mackenzie would like to thank the ARC for Large Grant A00103976 and the University of Sydney for their financial support and Geoscience Australia for access to their facilities. C.P.M and M.R.W

thank the Australian Research Council and Macquarie University for financial support.

References

1. Lambert IB, Scott KM (1973) J Geochem Explor 2:307–330
2. Legge PJ, Lambert IB (1994) Spec. Pub no. 10, Soc. Geol. Applied to Mineral Deposits. Springer, Heidleberg, pp 299-332
3. Large RR, Bull SW, Cooke DR, McGoldrick PJ (1998) Econ Geol 93:1345–1368
4. Large RR, Bull SW, McGoldrick PJ (2001) Econ Geol 96:1567–1593
5. Ireland T, Large RR, McGoldrick P, Blake M (2004) Econ Geol 99:1687–1709
6. Gustafson LB, Williams N (1981) Econ Geol 75th Anniversary volume, pp 139–178
7. Hinman MC (1996) James Cook University of North Queensland Economic Geology Research Unit, Extended Abstracts. Contribution 55:56–59
8. Walker RN, Logan RG, Binnekamp JG (1977) J Geol Soc Aust 24:365–380
9. Williams N, Logan RG (1981) Geol Soc Aust Abs 3:8
10. Muir MD (1983) Depositional environments of host rock to northern Australian lead-zinc deposits, with special reference to McArthur River. Mineralogical Association of Canada Short Course Handbook, vol 8, pp 141–147
11. Logan RG, Williams N (1984) Geol Soc Aust Abstr 12:339–340
12. Brown MC, Claxton CW, Plumb KA (1978) Bureau of Mineral Resources, Canberra, Record, 969/145, p 59
13. Bull SW (1998) Aust J Earth Sci 45:21–32
14. Logan GA, Hinman MC, Walter MR, Summons RE (2001) Geochim Cosmochim Acta 65:2317–2336
15. Chen J, Walter MR, Logan GA, Hinman MC, Summons RE (2003) Earth Planet Sci Lett 6636:1–13
16. Ireland T, Bull SW, Large R (2004) Miner Depos 39:143–158
17. Simoneit BRT (1984) Org Geochem 6:857–864
18. Simoneit BRT (1985) Hydrothermal petroleum: genesis, migration and deposition in Guaymas basin, Gulf of California. Can J Earth Sci 22:1919–1926
19. Simoneit BRT (1986) Geochimiya 11:236–254
20. Simoneit BRT, Fetzer JC (1996) Org Geochem 4:1065–1077
21. Simoneit BRT, Goodfellow WD, Franklin JM (1992) Appl Geochem 7:257–264
22. Simoneit BRT, Aboul-Kassim TAT, Tiercelin JJ (2000) Appl Geochem 15:355–368
23. Croxford NJW, Jephcott S (1972) Aust Inst Min Metall Proc 243:1–26
24. Logan RG (1979) The geology and mineralogical zoning of the HYC Ag–Pb–Zn deposit, McArthur River, Northern Territory, Australia. M.Sc. Thesis, Australia National University, Canberra
25. Lambert IB (1976) The McArthur zinc-lead-silver deposit: features, metallogenesis and comparisons with other stratiform ore. In: Wolf KH (ed) Handbook of Stratiform and Stratabound Ore Deposits.. Elsevier, Amsterdam pp 535–585
26. Eldridge CS, Williams N, Walsh JL (1993) Econ Geol 88:1–26
27. Smith, Croxford (1973) Nature Phys Sci 245:10–12
28. Williams N (1978) Econ Geol 73:1005–1035
29. Williams N (1978) Econ Geol 73:1036–1056
30. Durand B (1980) Kerogen: insoluable organic matter from sedimentary rocks. Paris, Editions Technip., pp 1–519
31. Eva Calvo, Carlos Pelegero, Grahma A. Logan (2003) J Chromatogr A 989:197–205
32. Chen J, Fu J, Sheng G, Liu D, Zhang J (1996) Org Geochem 25:179–190
33. Tuingstra F, Koenig JL (1970) J Chem Phys 53:1126–30
34. Katagiri G, Ishida H, Ishitani A (1988) Carbon 26:565–571
35. Wang Y, Alsmeyer DC, Mceery RL (1990) Chem Mater 2557–2563
36. Dresselhaus MS, Dresselhaus G (1981) Adv Phys 30:290–298
37. Zerda TW, John A, Chmura K (1981) Fuel 60:375–378
38. Nakamizo M, Kammereck R, Walker PJ (1974) Carbon 12:259–267
39. Al-Jishi , Dresselhaus (1982) Phys Rev B 26:4514–4522
40. Cuesta A, Dhamelincourt P, Laureyns J, Martinez-Alonso A, Tascon JMD (1994) Carbon 32:1523–32
41. Beny-Bassez C, Rouszaud JN (1985) Characterisation of carbonaceous materials by correlated electron and optical mioscopy and raman miospectroscopy. Scan Elect Miosc. 1:119–132
42. Hunt JM (1996) Petroleum geochemistry and geology, 2nd edn. W.H. Freeman and Company, New York, pp 1–389
43. Kawka OE, Simoniet BRT (1990) Appl Geochem 5:17–27
44. Simoneit BRT, (1994) Proceedings of the ocean drilling program, scientific results, vol 139, pp 447–465
45. Warner MC (1998) Geochemical characterization of sedimentary organic matter and hydrothermal petroleum in the black shale-hosted Zn–Pb deposit at Red Dog Mine, Western Brooks Range, Alaska. PhD Thesis, Indiana University
46. Puttman W, Hagemann HW, Merz C, Speczik S (1988) Org Geochem 13:357–363
47. Puttman W, Heppenheimer H, Diedel R (1990) Org Geochem 16:1145–1156
48. Simoneit BRT (1990) App Geochem 5:3–15
49. Hughes WB, Holba AG, Leon IPD (1995) Geochim Cosmochim Acta. 59:3581–3598
50. Radke DH, Welte DH, Willsch H (1986) Org Geochem 10: 51–63
51. Peters KE, Moldowan JM (1993) The biomarker guide—interpreting molecular fossils in petroleum and ancient sediments. Prentice–Hall, New Jersey, pp 1–363